COMMUNICATION

NOAH-(^{15}N/ ^{13}C)-CEST NMR Supersequence for Dynamics Studies of Biomolecules

Received 00th January 20xx,
Accepted 00th January 20xx

DOI: 10.1039/x0xx00000x

Rodrigo Cabrera Allpas,[a] Alexandar L. Hansen,[b] Rafael Brüschweiler[a,b,c*]

An NMR supersequence is introduced for the rapid acquisition of ^{15}N-CEST and methyl-^{13}C-CEST experiments in the same pulse sequence for applications to proteins. The high sensitivity and accuracy allows the simultaneous quantitative characterization of backbone and side-chain dynamics on the millisecond timescale ideal for routine screening for alternative protein states.

Conformational dynamics in biomolecules can occur on a wide range of timescales from picosecond to milliseconds and beyond and they often play a key role for protein function. Over the years, NMR has proven to be extraordinarily powerful to monitor and quantify the conformational dynamics of biomolecules at atomic detail.[1,2] An increasingly popular method is the Chemical Exchange Saturation Transfer (CEST) experiment, in which the spin magnetization is selectively saturated by a relatively long, weak radio-frequency (rf) pulse while conformational exchange occurs providing detailed information about lowly populated conformational states along with their Boltzmann population, chemical shifts, and kinetic exchange rates k_{ex} (typically from 20 to 200 s^{-1}).[3,4]

For biomolecular applications, CEST is performed as a pseudo-3D NMR experiment where the direct detection F2 dimension is along ^{1}H, the indirect F1 dimension is along the heteronucleus, such as ^{15}N or ^{13}C, and the pseudo-dimension is the frequency offset of the saturation field that is systematically sampled across the spectral range of interest. Hence, a CEST experiment involves the acquisition of many 2D ^{1}H-^{15}N or ^{1}H-^{13}C HSQC spectra, each of them being acquired with a saturation field applied using a variable frequency offset. The number of frequency offsets used along the pseudo-dimension can be rather large, usually in the hundreds, leading to prolonged measurements that can last between a day and a week per experiment depending on the sample concentration and NMR hardware used. Therefore, new approaches that substantially shorten this process are needed.

Recently, a strategy to acquire multiple NMR experiments in sequence has been introduced, known as "NMR by Ordered Acquisition using ^{1}H detection" or NOAH.[5] NOAH combines multiple homo- and hetero-nuclear 2D NMR experiments in a single pulse sequence resulting in a "supersequence" where a single recovery delay is placed between sets of scans, thereby significantly reducing the experimental time when compared with the standalone pulse experiments that require a recovery delay after each scan (see also **Fig 1**).[5–9] So far, NOAH has been mostly applied to small organic molecules in concentrated purified samples combining sets of experiments used for resonance assignments and molecular structure elucidation.[6] NOAH has also been extended to complex metabolomics mixture analysis.[10,11] For proteins, sequential acquisition of correlation spectra has been reported for resonance assignments.[12,13] As of now, the NOAH strategy has not been utilized to benefit protein dynamics experiments.

A critical prerequisite for NOAH is the need to preserve magnetization for the immediately succeeding pulse sequence inside the supersequence in order to guarantee good sensitivity.[5] Applications of NOAH to small organic molecules have been conducted at ^{13}C natural abundance. For example, using 1.1% of ^{1}H magnetization bound to a ^{13}C nucleus for an HSQC-type experiment and using the remaining 98.9% ^{1}H magnetization for a homonuclear experiment such as TOCSY, as the second experiment, will result in a HSQC/TOCSY supersequence. In addition, specific pulse sequence elements, such as ZIP[10] and ASAP,[14] are useful to preserve or recover magnetization in NOAH sequences used as starting points in subsequent experiments.[6] An advantage of NOAH is that each individual standalone sequence typically requires only minor modifications inside the supersequence resulting in spectra that closely resemble those of the corresponding standalone sequences. Another advantage is that most NMR pulse sequence parameters remain unchanged when a sequence is incorporated into a supersequence, thereby facilitating both testing and application.

[a] *Department of Chemistry and Biochemistry, The Ohio State University, Columbus, Ohio 43210, U.S.A.*
[b] *Campus Chemical Instrument Center, The Ohio State University, Columbus, Ohio 43210, U.S.A.*
[c] *Department of Biological Chemistry and Pharmacology, The Ohio State University, Columbus, Ohio 43210, U.S.A.*

† Electronic Supplementary Information (ESI) available: Details of the NOAH-(^{15}N/^{13}C)-CEST sequence and details of the acquisition of the experiments and methods employed. See DOI: 10.1039/x0xx00000x

Here, we introduce a new supersequence, which was created by concatenating a ^{15}N-CEST and a ^{13}C-CEST for the purpose of studying protein dynamics in biomolecules along the backbone (^{15}N-CEST) and in the methyl groups of amino-acid side-chains (^{13}C-CEST) (**Figs 1, S1**). We refer to this supersequence as *NOAH-(^{15}N/^{13}C)-CEST*. Results of the standalone ^{15}N-CEST and ^{13}C-CEST experiments are first presented and compared against a supersequence built from these individual sequences for the colicin E7 immunity protein (Im7) and ubiquitin. Since protein NMR samples are prepared in uniformly ^{15}N and ^{13}C-labeled form, some of the NOAH strategies successfully used for small organic molecules at natural abundance do not apply. Here, we start with the ^{15}N-CEST experiment during which ^{13}C magnetization is preserved and used as starting magnetization for the following ^{13}C-CEST during the 2nd half of the supersequence. We show that both ^{15}N-CEST and the ^{13}C-CEST have good sensitivity despite using thermal ^{13}C starting magnetization for the second part of the sequence when compared to a regular standalone ^{13}C-CEST using ^{1}H starting magnetization. The resulting CEST profiles and CEST fitting results are then compared with those of the standalone sequences.

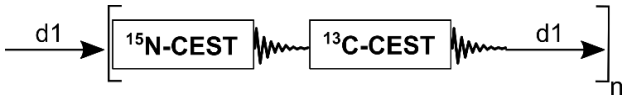

Figure 1. Modular representation of the NOAH-(^{15}N/^{13}C)-CEST supersequence. Delay *d1* is the recovery delay and n is the number of times the sequence is repeated. The ^{15}N-CEST module starts with ^{1}H magnetization, while the ^{13}C-CEST module starts with thermal ^{13}C magnetization, which remains unperturbed during the first module. The complete pulse sequence is depicted in Fig S1.

By preserving ^{13}C magnetization during ^{15}N-CEST, the ^{13}C-CEST can immediately follow without any relaxation delay as implemented in the supersequence scheme of **Fig 1**. The ^{13}C magnetization employed is at thermal equilibrium and proportional in size to the gyromagnetic ratio (compared to ^{1}H, γ_C/γ_H = ¼). It therefore does not originate from ^{1}H magnetization by an INEPT-type transfer used in standard ^{13}C-CEST. In the context of NOAH, this has the advantage that the starting ^{13}C magnetization of the 2nd experiment is not affected by depletion of ^{1}H magnetization during the course of the 1st experiment. To assess the sensitivity of this "^{13}C-start" ^{13}C-CEST with the standard ^{13}C-CEST, we measured it both as a standalone experiment and as the 2nd part of the supersequence of **Fig 1**. All NMR experiments were performed with a *d1* of 2 s on an 850 MHz Bruker Ascend magnet equipped with an Avance III HD console and a triple resonance inverse cryoprobe and processed using NMRPipe.[15] The standalone direct ^{13}C-CEST and direct ^{13}C-CEST in the supersequence have on average, based on average cross-peak amplitudes determined by cross-peak fitting for ubiquitin and Im7, a 16% and 11% lower sensitivity than the standard ^{13}C-CEST experiment, respectively. The loss of sensitivity for the ^{15}N-CEST when being part of the supersequence was on average 12% and 7% for ubiquitin and Im7, respectively compared to the standalone ^{15}N-CEST. For Im7, the ^{15}N-CEST experiment was acquired in 38 hours and the ^{13}C-CEST experiment in 36 hours, for a total of 74 hours for both experiments together. By comparison, the NOAH-(^{15}N/^{13}C)-CEST experiment, including both ^{15}N-CEST and ^{13}C-CEST, was acquired in 45 hours. Therefore, the supersequence produced both experiments, but in 29 hours less time corresponding to 39% saving of spectrometer time. Even if the supersequence is ran longer to have ^{13}C-CEST sensitivity equivalent to that of the standalone sequence, there is still a substantial net gain in experiment time, while the ^{15}N-CEST experiment will have better sensitivity than the reference experiment. The average signal-to-noise ratios along with the experiment times of each sequence are summarized in **Table 1**.

Table 1. Signal-to-noise ratios of ^{15}N-CEST, ^{13}C-CEST and NOAH-(^{15}N/^{13}C)-CEST experiments, and their individual measurement time for Im7.

Experiment	S/N[c]	Individual measurement time (hrs)	Combined measurement time (hrs)
^{15}N-CEST	205	38	74
^{13}C-CEST[a]	179	36	
^{13}C-CEST[b]	156	42	80
NOAH ^{15}N-CEST	191	-	45
NOAH ^{13}C-CEST	160		

[a] Standard ^{13}C-CEST with starting ^{1}H magnetization.

[b] Modified ^{13}C-CEST with starting ^{13}C magnetization and additional ^{1}H decoupling pulses.

[c] Average S/N for all non-overlapping protein cross-peaks.

The standalone ^{13}C-CEST with starting ^{13}C magnetization has the same sensitivity as the one in the supersequence, which shows that the addition of heat compensation pulses, implemented as decoupling pulse trains applied to ^{1}H, results in an increase in sensitivity when using the ^{13}C magnetization as starting magnetization. This is likely caused by the concurrent heteronuclear Overhauser effect (hetNOE) enhancement via cross-relaxation of ^{1}H to ^{13}C magnetization within the methyl groups during the heat compensation pulses. As can be seen in **Table 1**, the addition of ^{1}H decoupling pulses to the modified ^{13}C-CEST with ^{13}C starting magnetization leads to a similar sensitivity as the ^{13}C-CEST in the supersequence and it is not far below the signal-to-noise ratio obtained with a regular ^{13}C-CEST with ^{1}H starting magnetization. This enhancement is notable as it opens the possibility of incorporating other methyl-^{13}C-start pulse sequences into other types of supersequences.

After having established that the new supersequence for ^{15}N-CEST and ^{13}C-CEST saves experiment time with only minor sensitivity loss, we tested whether the information obtained by these NOAH-(^{15}N/^{13}C)-CEST profiles is identical to what is obtained by the standalone experiments. **Fig 2** compares CEST profiles of selected residues of Im7 for ^{15}N-CEST with no conformational exchange (top) or two-site exchange (bottom). It demonstrates that the CEST profiles obtained by the two methods are identical. Even small features, such as the shoulder peak of Arg61 on the left of the main dip can be accurately reproduced.

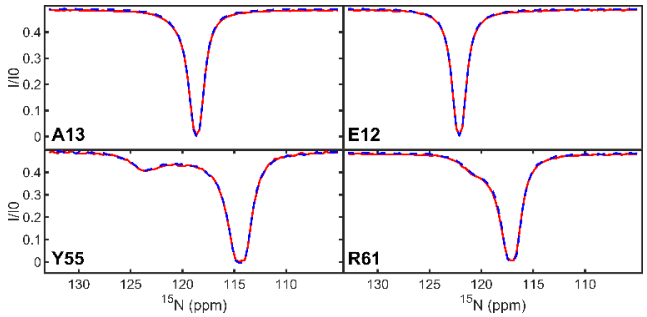

Figure 2. Representative ^{15}N-CEST profiles for Im7 residues A13, E12, Y55, and R61 from the supersequence (red, solid line) and the standalone sequence (blue, dashed line). Top panels show residues without exchange and the bottom panels show residues that undergo two-site exchange with a 2nd minimum or "shoulder" feature visible in the profile.

The analogous comparison is shown for ^{13}C-CEST in **Fig 3**. As for ^{15}N-CEST, the profiles are identical for the standalone experiment vs. supersequence. Small decoupling sidebands can be seen in the bottom panels, which slightly vary since different decoupling sequences were used. Moreover, it can be seen in the bottom panels that the supersequence is able to highly accurately reproduce two-site exchange features manifested as shoulder peaks.

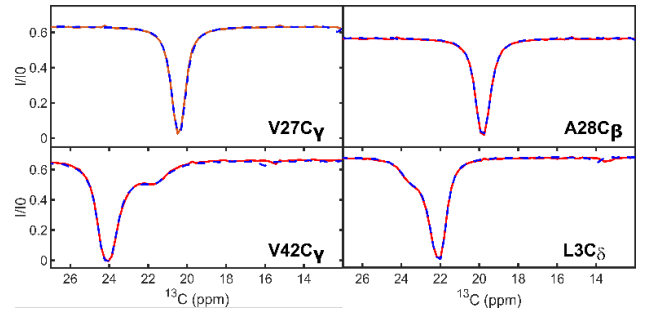

Figure 3. Representative ^{13}C-CEST profiles for Im7 residues V27C$_\gamma$, A28C$_\beta$, V42C$_\gamma$, and L3C$_\delta$ from the supersequence (red, solid line) and the standalone sequence (blue, dashed line). Top panels show residues without exchange and the bottom panels show residues that undergo two-site exchange with a 2nd minimum or "shoulder" feature clearly visible in the profile.

From the CEST profiles, relaxation and exchange model parameters were extracted using ChemEx (http://www.github.com/gbouvignies/chemex)[3] by non-linear least squares fitting and quantitatively compared with the model parameters between the sequences. The parameters extracted are the longitudinal and transverse relaxation rates R_1 and R_2 of the major state and in the case of two-site exchange also ΔΩ (chemical shift difference between the two states), p_A (population of major state) and the exchange rate constant $k_{ex} = k_{forward} + k_{reverse}$. **Fig 4** shows a correlation plot between the fitting results for ΔΩ, R_1 and R_2 of the major state based on the standalone ^{15}N-CEST and the NOAH ^{15}N-CEST for Im7. Residues with strong overlap were not included in the analysis. Linear regression yields a slope close to 1 with a very small intercept and a high correlation coefficient reflecting the equivalence between the fitting results for the standalone and the supersequence. For the 2-site exchange model applied to the CEST profiles obtained with the standalone ^{15}N-CEST, the fitted p_A and k_{ex} values were 0.99 and 853 s^{-1}, respectively, while for the NOAH ^{15}N-CEST, these parameters were 0.99 and 757 s^{-1}, respectively. For the standalone ^{13}C-CEST, the fitted p_A and k_{ex} values were 0.99 and 664 s^{-1}, respectively, while for the NOAH ^{13}C-CEST, these parameters were 0.99 and 644 s^{-1}, respectively. In practice, by measuring CEST profiles at a second B_1 field, as is frequently done, robustness of the fitting results should improve and thereby further decrease the difference between the fitted model parameters.

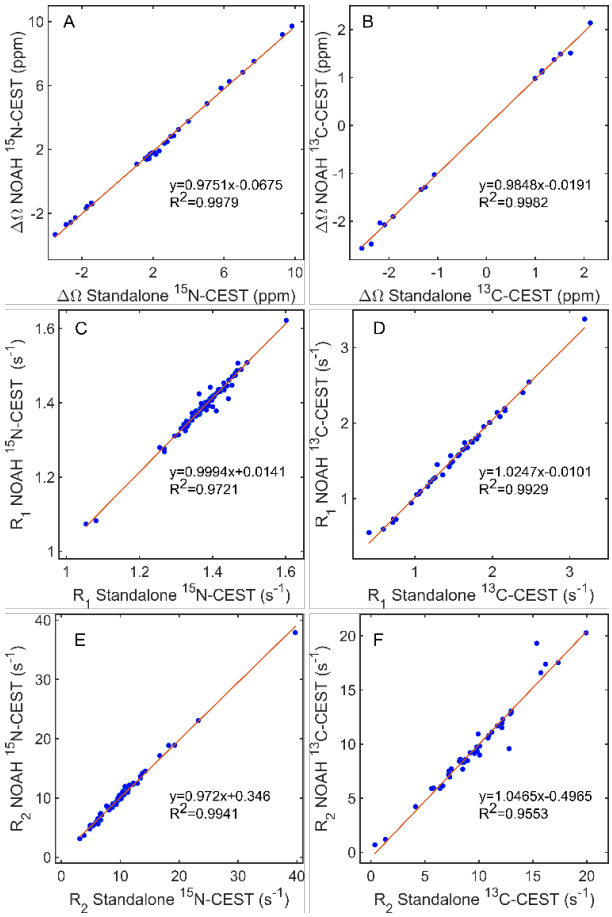

Figure 4. Correlation plots between standard standalone and the NOAH-(^{15}N/^{13}C)-CEST supersequence for Im7, A) ΔΩ standalone ^{15}N-CEST vs ΔΩ NOAH ^{15}N-CEST, B) ΔΩ standalone ^{13}C-CEST vs ΔΩ NOAH ^{13}C-CEST, C) R_1 standalone ^{15}N-CEST vs R_1 NOAH ^{15}N-CEST, D) R_1 standalone ^{13}C-CEST vs R_1 NOAH ^{13}C-CEST, E) R_2 standalone ^{15}N-CEST vs R_2 NOAH ^{15}N-CEST, F) R_2 standalone ^{13}C-CEST vs R_2 NOAH ^{13}C-CEST. The linear regression relationships together with Pearson correlation coefficients R^2 are displayed in each panel.

In principle, the experimental parameters used to run a NOAH-(^{15}N/^{13}C)-CEST experiment in a ^{15}N and ^{13}C-labeled protein are the same as those when each sequence is executed as a standalone sequence, which facilitates the implementation of the CEST supersequence introduced here. A constraint of this experiment is that both ^{15}N and ^{13}C-CEST supersequence blocks use the same number of rf offsets. Alternatively, it is possible to perform one CEST block with half (or one third) the number of rf offsets compared to the other by repeating for one CEST block the same offset twice (or

three times). In practice, however, this limitation should be immaterial as it is outweighed by the substantial time saving allowing one to obtain the entire ^{13}C-CEST experiment essentially for free. Average ^{13}C-T_1 relaxation times of Im7 and ubiquitin were 0.62 ± 0.33 s. Larger proteins with longer T_1's will require a longer recovery delay *d1* (**Fig 1**), but the relative time saving with respect to standalone CEST experiments will remain.

An attractive application of the NOAH-(^{15}N/^{13}C)-CEST supersequence is the high-throughput screening of protein dynamics, for example, to analyze proteins in the absence vs the presence of ligands (complex) or wild-type vs a mutant protein,[16] where it will substantially reduce the NMR time when both backbone and side-chain properties are of interest. Furthermore, it has been shown that using CEST-derived ^{15}N R_1 and R_2 exchange parameters a lean model-free approach (L-MFA) can be applied for the extraction of S^2 order parameters with high accuracy.[17] Considering that the supersequence results are equivalent to those of standalone CEST, the supersequence not only provides information about conformational substates exchanging on the ms time scale, but also on the ps – ns timescale reflected in S^2 order parameters. This promises to further speed up NMR measurement time for the comprehensive characterization of protein dynamics on time scales from ps to ms for both the protein backbone and side-chains.[17]

In summary, extended experiment times, which poses a significant bottleneck for pseudo-3D NMR experiments to study biomolecular dynamics of both backbone and side-chain moieties, has been addressed here using the NOAH strategy by combining the ^{15}N-CEST and ^{13}C-CEST into one supersequence. This allows time savings of about 39%, or more than an entire day, when compared to running these sequences in their traditional standalone mode. This new supersequence makes CEST experiments amenable for the screening of protein dynamics under variable experimental conditions, such as temperature, buffer, ligands, or pressure, for the more rapid identification of mutants or substrates of interest involving dynamics changes along the backbone and the side-chains. Furthermore, we showed that the resulting CEST profiles obtained from standalone and NOAH-(^{15}N/^{13}C)-CEST experiments are identical (**Figs 2, 3**), leading to accurate CEST fitting results both in the absence and presence of exchange **(Fig 4**). Given the nature of some biomolecules to degrade over time, the application of NOAH for CEST experiments could prove to be a valuable alternative for measuring backbone and side-chain dynamics in significantly less time. Moreover, longer acquisition times can also be more affected by temperature variations, shimming effects, and other fluctuations, which the supersequence could help mitigate. The combination of NOAH-(^{15}N/^{13}C)-CEST with other time-saving techniques, such as multi-frequency excitation,[18,19] and non-uniform[20] and absolute minimal sampling[21] should result in even faster acquisition times. For NOAH experiments of small organic molecules, the computer-assisted generation of supersequences from a library of common NMR experiments has recently been introduced.[22] As NOAH experiments start being explored for biomolecular NMR applications, this type of approach may be also feasible for the modular, customized design of new experiments.

This work was supported by the U.S. National Science Foundation (grant MCB-1715505 to R.B.). All NMR experiments were performed at the Campus Chemical Instrument Center NMR facility at Ohio State University.

Rodrigo Cabrera Allpas: Developed pulse sequence, Analyzed results, Wrote original manuscript draft; **Alexandar L. Hansen**: Developed pulse sequence, Advised on analysis, Edited manuscript; **Rafael Brüschweiler**: Conceived project, Wrote manuscript, Managed project.

There are no conflicts to declare

Notes and references

1 T. R. Alderson and L. E. Kay, *Cell*, 2021, **184**, 577–595.
2 A. G. Palmer and H. Koss, in *Methods in Enzymology*, ed. A. J. Wand, Academic Press, 2019, vol. 615, pp. 177–236.
3 P. Vallurupalli, G. Bouvignies and L. E. Kay, *J. Am. Chem. Soc.*, 2012, **134**, 8148–8161.
4 P. Vallurupalli, A. Sekhar, T. Yuwen and L. E. Kay, *J. Biomol. NMR*, 2017, **67**, 243–271.
5 Ē. Kupče and T. D. W. Claridge, *Angew. Chem. Int. Ed.*, 2017, **56**, 11779–11783.
6 T. D. W. Claridge, M. Mayzel and Ē. Kupče, *Magn. Reson. Chem.*, 2019, **57**, 946–952.
7 Ē. Kupče and T. D. W. Claridge, *J. Magn. Reson.*, 2019, **307**, 106568.
8 Ē. Kupče and T. D. W. Claridge, *Chem. Commun.*, 2018, **54**, 7139–7142.
9 Ē. Kupče, J. R. J. Yong, G. Widmalm and T. D. W. Claridge, *JACS Au*, 2021, **1**, 1892–1897.
10 A. L. Hansen, E. Kupče, D.-W. Li, L. Bruschweiler-Li, C. Wang and R. Brüschweiler, *Anal. Chem.*, 2021, **93**, 6112–6119.
11 F. Tang and E. Hatzakis, *Anal. Chem.*, 2020, **92**, 11177–11185.
12 P. Bellstedt, Y. Ihle, C. Wiedemann, A. Kirschstein, C. Herbst, M. Görlach and R. Ramachandran, *Sci. Rep.*, 2014, **4**, 4490.
13 C. Wiedemann, P. Bellstedt, A. Kirschstein, S. Häfner, C. Herbst, M. Görlach and R. Ramachandran, *J. Magn. Reson.*, 2014, **239**, 23–28.
14 E. Kupče and R. Freeman, *Magn. Reson. Chem.*, 2007, **45**, 2–4.
15 F. Delaglio, S. Grzesiek, G. W. Vuister, G. Zhu, J. Pfeifer and A. Bax, *J. Biomol. NMR*, 1995, **6**, 277–293.
16 T. Xie, T. Saleh, P. Rossi and C. G. Kalodimos, *Science*, 2020, **370**, eabc2754.
17 Y. Gu, A. L. Hansen, Y. Peng and R. Brüschweiler, *Angew. Chem. Int. Ed.*, 2016, **55**, 3117–3119.
18 T. Yuwen, L. E. Kay and G. Bouvignies, *ChemPhysChem*, 2018, **19**, 1707–1710.
19 M. Leninger, W. M. Marsiglia, A. Jerschow and N. J. Traaseth, *J. Biomol. NMR*, 2018, **71**, 19–30.
20 G. Jameson, A. L. Hansen, D. Li, L. Bruschweiler-Li and R. Brüschweiler, *J. Am. Chem. Soc.*, 2019, **141**, 16829–16838.
21 K. Kazimierczuk and V. Orekhov, *Magn. Reson. Chem.*, 2015, **53**, 921–926.
22 J. R. J. Yong, E. Kupče and T. D. W. Claridge, *Anal. Chem.*, 2022, **94**, 2271–2278.

